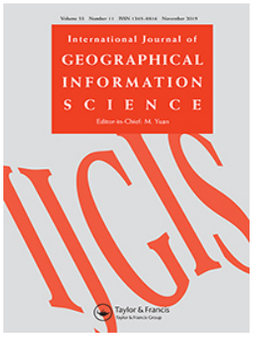

International Journal of Geographical Information Science

ISSN: 1365-8816 (Print) 1362-3087 (Online) Journal homepage: https://www.tandfonline.com/loi/tgis20

Uncertain seas: probabilistic modeling of future coastal flood zones

Christopher J. Amante

To cite this article: Christopher J. Amante (2019) Uncertain seas: probabilistic modeling of future coastal flood zones, International Journal of Geographical Information Science, 33:11, 2188-2217, DOI: 10.1080/13658816.2019.1635253

To link to this article: https://doi.org/10.1080/13658816.2019.1635253

Published online: 08 Jul 2019.

INTERNATIONAL JOURNAL OF GEOGRAPHICAL INFORMATION SCIENCE
2019, VOL. 33, NO. 11, 2188–2217
https://doi.org/10.1080/13658816.2019.1635253

Taylor & Francis
Taylor & Francis Group

RESEARCH ARTICLE

OPEN ACCESS Check for updates

Uncertain seas: probabilistic modeling of future coastal flood zones

Christopher J. Amante

Cooperative Institute for Research in Environmental Sciences, University of Colorado Boulder, Boulder, CO, USA; National Oceanic and Atmospheric Administration, National Centers for Environmental Information, Boulder, CO, USA

ABSTRACT

Future sea-level rise will likely expand the inland extent of storm surge inundation and, in turn, increase the vulnerability of the people, properties and economies of coastal communities. Modeling future storm surge inundation enhanced by sea-level rise uses numerous data sources with inherent uncertainties. There is uncertainty in (1) hydrodynamic storm surge models, (2) future sea-level rise projections, and (3) topographic digital elevation models representing the height of the coastal land surface. This study implemented a Monte Carlo approach to incorporate the uncertainties of these data sources and model the future 1% flood zone extent in the Tottenville neighborhood of New York City (NYC) in a probabilistic, geographical information science (GIS) framework. Generated spatiotemporal statistical products indicate a range of possible future flood zone extents that results from the uncertainties of the data sources and from the terrain itself. Small changes in the modeled land and water heights within the estimated uncertainties of the data sources results in larger uncertainty in the future flood zone extent in low-lying areas with smaller terrain slope. An interactive web map, UncertainSeas.com, visualizes these statistical products and can inform coastal management policies to reduce the vulnerability of Tottenville, NYC to future coastal inundation.

ARTICLE HISTORY
Received 19 December 2018
Accepted 19 June 2019

KEYWORDS
Sea-level rise; storm surge inundation; digital elevation model; uncertainty; probabilistic coastal flood model

Introduction

The rate of global sea-level rise will likely increase due to increases in ocean temperature and increases in land-ice melt (Parris *et al*. 2012, Church 2013). Coastal properties are already prone to flooding and coastal flooding is expected to be exacerbated by future sea-level rise (Wong *et al*. 2014, Sweet *et al*. 2017, Fleming 2018). In 2012, Superstorm Sandy resulted in approximately $19 billion in damage and 48 lives lost in New York City (NYC, Blake *et al*. 2013). There were two deaths in the Tottenville neighborhood of NYC during Superstorm Sandy, and this neighborhood is the case study for modeling future flood zones from storm surge inundation enhanced by sea-level rise.

Sea-level rise in NYC has already increased the number and magnitude of coastal flood events (Sweet *et al*. 2013, Talke *et al*. 2014), and coastal flood zones will likely

CONTACT Christopher J. Amante Christopher.Amante@colorado.edu; Christopher.Amante@noaa.gov

expand in NYC in the future (Horton *et al*. 2015). Sea-level rise is a relatively slow process, however, it will likely continue to increase the frequency, magnitude, and duration of storm surge inundation (Parris *et al*. 2012). Future storm surge inundation enhanced by sea-level rise will, in turn, likely increase the vulnerability of the people, properties and economy of NYC.

Modeling future storm surge inundation enhanced by sea-level rise uses numerous data sources with inherent uncertainties. There is uncertainty in (1) hydrodynamic storm surge models, (2) future sea-level rise projections, and (3) topographic digital elevation models (DEMs) representing the height of the coastal land surface above established vertical datums. This study implements a Monte Carlo approach to incorporate the uncertainties of these data sources and model the future 1% flood zone extent in the Tottenville neighborhood of NYC in a probabilistic, geographical information science (GIS) framework.

Literature review

The following sections provide background information on storm surge, sea-level rise, and DEMs, and their inherent uncertainties, as well as previous research on modeling future storm surge inundation enhanced by sea-level rise.

Storm surge

Storm surge is the build-up of water onto coastal land from wind shear stress associated with intense low-pressure weather systems, such as tropical and extratropical cyclones (Murty *et al*. 1986). Present-day coastal flood zones from storm surge inundation are typically determined by hydrodynamic models including the Sea, Lake, and Overland Surges from Hurricanes (SLOSH, Jelesnianski *et al*. 1992) and the ADvanced CIRCulation (ADCIRC, Luettich *et al*. 1992) models.

Many studies use hydrodynamic models, such as SLOSH and ADCIRC, *directly* to delineate potentially inundated areas (*e.g*., McInnes *et al*. 2003, 2013, Kleinosky *et al*. 2007, Frazier *et al*. 2010, Shepard *et al*. 2012, Atkinson *et al*. 2013, Ding *et al*. 2013, Zhang *et al*. 2013, Maloney and Preston 2014). Other coastal inundation studies use products *derived* from storm surge model outputs, such as the Federal Emergency Management Agency (FEMA) Flood Insurance Rate Maps (FIRMs, *e.g*., Patrick *et al*. 2015). FEMA FIRMs are typically derived from outputs from ADCIRC and coupled wave models, such as the Simulating WAves Nearshore (SWAN) model (Algeo and Mahoney 2011, FEMA 2014, Kress *et al*. 2016). FIRMs determine flood insurance rates based on the 1% annual chance of inundation and identify where flood insurance is required as a condition of a federally-backed mortgage (Burby 2001).

Sources of uncertainty in storm surge models and, consequently, in derived products such as FEMA FIRMs, originate from the input parameters, including wind speed and direction, bathymetry, topography, friction coefficients, and boundary conditions (Atkinson *et al*. 2013). There is also uncertainty in the historical meteorological data on extreme events and the choice of statistical functions that represent their occurrence (McInnes *et al*. 2003).

Sea-level rise

Sea-level rise provides an elevated water base for storm surge to build on, and future sea-level rise will likely continue to increase the frequency, magnitude, and duration of storm surge inundation (Parris *et al*. 2012). Coastal flooding occurs at the land-water interface, and, therefore, local information on the relative vertical movement between the land and water surface is required to model future flood zones. Local sea-level projections can diverge from the global mean due to differences in ocean temperature, salinity, currents, and land elevation changes due to glacial isostatic adjustment, human extraction of ground water, and tectonic processes (Nerem and Mitchum 2001, Cazenave and Nerem 2004, Lombard *et al*. 2005, Milne *et al*. 2009, Church 2013). Relative sea-level rise in NYC is expected to exceed the global average primarily due to local land subsidence and to increases in regional sea-level, due in part to projected weakening of the Gulf Stream current (Yin *et al*. 2009, 2010, Kenigson and Han 2014, Horton *et al*. 2015).

Other regional factors that can affect future sea-level in NYC include climate modes, such as the North Atlantic Oscillation (NAO, Barnston and Livezey 1987, Hurrell 1995, Kopp 2013, Han *et al*. 2017) and the Atlantic Multidecadal Oscillation (AMO, Trenberth and Shea 2006, Wang and Zhang 2013, Han *et al*. 2017). Han *et al*. (2017) identified limitations of understanding regional sea-level change, including representation of these climate modes, interactions among climate modes, effects of anthropogenic forcing on the modes, effects of ocean internal variability, and limited observational records. These limitations must be addressed to fully understand the climate modes' impact on regional sea-level, and to reduce uncertainty in future sea-level rise projections (Han *et al*. 2017).

Digital elevation models (DEMs)

The topographic elevation above sea-level is a primary factor that determines the inland extent of coastal flooding. Accordingly, one of the most common methods for modeling coastal inundation is 'bathtub modeling.' Bathtub modeling delineates flood zones as areas where coastal land elevation values are below a modeled water height that represents a sea-level rise projection and/or storm surge level (*e.g*., Poulter and Halpin 2008, Gesch 2009, 2012, 2013, Leon *et al*. 2014, Schmid *et al*. 2014, West *et al*. 2018). Different representations of the topographic elevations, consequently, can result in large differences in the modeled flood zones (Coveney and Fotheringham 2011, Zhang 2011, West *et al*. 2018), especially for low-lying coastal areas (Van de Sande *et al*. 2012). Estimations of potential DEM errors, *i.e*., DEM uncertainty, should, therefore, be incorporated in flood models to produce a range of possible flood zones.

DEMs can be generated from various data sources and methods (Nelson *et al*. 2009, Wilson 2012, Maune and Nayegandhi 2018), including traditional ground-surveys with theodolites (Nelson *et al*. 2009), satellite-derived stereo photogrammetry (Shean *et al*. 2016, Almeida *et al*. 2019), structure-from-motion (Mancini *et al*. 2013), radio detection and ranging (RADAR) interferometry (Rabus *et al*. 2003), and light detection and ranging (LIDAR, Maune and Nayegandhi 2018). These various data sources and methods result in DEMs with different spatial resolutions and vertical accuracies (Nelson *et al*. 2009).

Furthermore, coastal DEMs are often generated by integrating numerous elevation data sources of disparate age, quality and measurement density (Eakins and Taylor 2010, Eakins and Grothe 2014, Amante 2018b), resulting in spatially-varying vertical uncertainty (Amante 2018b).

Modeling future storm surge inundation enhanced by sea-level rise

There are two general methodologies to model future storm surge inundation enhanced by sea-level rise: dynamic (also known as hydrodynamic or numerical simulation) and static (also known as bathtub) modeling. Dynamic modeling evaluates sea-level rise projections, and changes storm surge and wave model input variables, such as ocean depths and bottom friction coefficients, *before* modeling storm surge (Atkinson *et al*. 2013, Zhang *et al*. 2013, Orton *et al*. 2015).

Conversely, static modeling evaluates sea-level rise projections *after* obtaining the output from present-day storm surge and wave models, or indirectly, such as with the present-day FEMA FIRM 1% flood zone, in a GIS framework (Zhang *et al*. 2013, Leon *et al*. 2014, Patrick *et al*. 2015). The static, linear addition by expansion method adds a sea-level rise increment to the present-day modeled storm surge heights. The future storm surge inundation area is then delineated as areas where the cumulative water levels are greater than the DEM values (McInnes *et al*. 2013, Zhang *et al*. 2013). The linear addition by expansion method does not incorporate physical forces on the water movement considered in dynamic modeling, such as differences in bottom friction due to changing water depths and landscape characteristics. However, the linear addition by expansion method more closely mimics the results of dynamic methods compared to other static methods (Zhang *et al*. 2013).

Inland local depressions that have elevations below a projected water level and are not connected to the ocean are incorrectly inundated in GIS-based, static methods that do not implement water connectivity algorithms (*e.g*., Titus and Richman 2001). In these cases, terrain barriers exist between the ocean and the low-lying areas that would prevent inundation (Li *et al*. 2009). In studies that implement water connectivity algorithms, areas are considered inundated only where their elevations are less than the modeled water levels and are also adjacent to the current or modeled future ocean area (*e.g*., Poulter and Halpin 2008, Gesch 2009, Li *et al*. 2009, Zhang *et al*. 2013). Adjacency is typically defined by either 4 or 8 neighbors in a 3×3 kernel. The 4-neighbor case only considers the 4 cardinal directions (*i.e*., N, E, S, W), and the 8-neighbor case considers all adjacent cells (*i.e*., N, NE, E, SE, S, SW, W, NW).

Dynamic methods of modeling future storm surge inundation enhanced by sea-level rise are more complex than GIS-based, static methods, which results in larger computational expense. Consequently, dynamic methods typically cannot simulate numerous sea-level rise projections, storm surge scenarios, and DEM realizations to incorporate the uncertainties of these data sources (Orton *et al*. 2015). Zhang *et al*. (2013) found that dynamic methods require approximately 30 to 60 times more computation time than the static linear addition by expansion method to model future storm surge inundation enhanced by a given sea-level rise projection. Therefore, computational expense is greatly reduced if static methods can approximate dynamic methods of modeling future coastal flood zones (Zhang *et al*. 2013).

GIS-based, static methods assume storm surge inundation dynamics are the same with current and future sea-levels, and the enhanced storm surge heights are simply the linear addition of the present-day storm surge heights and the future sea-level rise. However, the relationship between storm surge heights and sea-level rise can be non-linear in shallow water due to changes in bottom friction and shoreline configuration (Lowe *et al*. 2001, Lowe and Gregory 2005, Loder *et al*. 2009, Ding *et al*. 2013, Zhang *et al*. 2013).

There are a few, notable studies that directly compare the results of dynamic and GIS-based, static modeling of future coastal inundation (*e.g*., Zhang *et al*. 2013, Orton *et al*. 2015, Patrick *et al*. 2015, Seenath *et al*. 2016). Zhang *et al*. (2013) determined that inundation areas and peak storm surge heights generated by the static, linear addition by expansion method differed from the dynamic method by only 7% and 4% on average, respectively. Seenath *et al*. (2016) also determined that a GIS-based, static method produced an inundation area that was within 5% of dynamic methods.

Two studies modeled future storm surge inundation enhanced by sea-level rise in NYC to compare GIS-based, static methods (Patrick *et al*. 2015) and dynamic methods (Orton *et al*. 2015). The static and dynamic methods resulted in similar storm surge heights for most locations (usually within approximately ± 0.15-m) and resulted in similar future flood zone boundaries (Orton *et al*. 2015). The main purpose of these NYC studies was to compare static and dynamic methods, however, both studies acknowledged limitations due to the lack of incorporation of input data uncertainties into their analyses. Specifically, Patrick *et al*. (2015) stated estimates of uncertainty associated with the elevation, sea-level rise, and FEMA flood heights should be used to determine the degree of confidence in the flood model outputs.

Lin *et al*. (2012) also determined that static methods were an excellent approximation of dynamic methods in NYC. The bottom friction is expected to remain relatively constant under future sea-level rise in urban areas, where the existing land cover is not dominated by vegetation, and, consequently, the effect of changes to bottom friction is expected to be minor compared to the effect of the water level increase from sea-level rise (Atkinson *et al*. 2013). These previous studies indicate that GIS-based, static methods can approximate dynamic modeling of future flood zones in NYC. Importantly, static methods enable the incorporation of input data uncertainties to determine the likelihood of the future flood zone extent in a probabilistic framework, which would be computationally impractical with dynamic methods.

Probabilistic future flood models

Deterministic flood models that do not consider input data uncertainties can result in inaccurate and misleading future coastal flood zones, and potentially inappropriate coastal management policies (West *et al*. 2018). Probabilistic flood models that consider these data uncertainties can reduce the conveyed over-confidence of a single, deterministic flood model, demonstrate the effect of data uncertainties on the flood model, and produce a range of possible alternative flood model outcomes (Cowell *et al*. 2006, Hare *et al*. 2011, Wallentin and Car 2013, Winter *et al*. 2018). Flood models should, therefore, incorporate the uncertainties in storm surge models, sea-level rise projections, and DEMs in a probabilistic framework to determine future coastal flood zones. Probabilistic flood

models can then inform coastal management policies by indicating the likelihood of the future flood zone extent.

Several previous studies modeled future flood zones by incorporating the uncertainty in one or two of the major sources of input data, *i.e.*, present-day storm surge, sea-level rise projections, and DEM (*e.g.*, Gesch 2009, 2012, 2013, Li *et al*. 2009, Neumann *et al*. 2010, Zhang 2011, Strauss *et al*. 2012, Albert *et al*. 2013, Cooper and Chen 2013, Leon *et al*. 2014, Schmid *et al*. 2014, Kane *et al*. 2015, West *et al*. 2018). There is limited research on modeling future storm surge inundation enhanced by sea-level rise that incorporates these three major sources of uncertainty in a probabilistic framework. Furthermore, almost all previous studies focused on the spatial uncertainty of inundation extent that results from the uncertainties of these data sources. One notable exception, Kane *et al*. (2015), determined the time frame when sea-level rise could result in a rapid increase in areas prone to flooding.

Leon *et al*. (2014) incorporated DEM uncertainty in modeling the combined effect of a uniform 1% storm surge height of 2.9-m and a 1-m sea-level rise projection. Leon *et al*. (2014) improved the incorporation of DEM uncertainty in coastal flood models by spatially distributing DEM errors based on land cover and terrain variables. Specifically, Leon *et al*. (2014) quantified vertical errors as differences between the DEM and more accurate real-time kinematic (RTK) GPS elevation measurements. The errors were then correlated with land cover and terrain variables and 1,000 vertical error surfaces were generated using sequential Gaussian simulations and regression-kriging in a Monte Carlo, probabilistic approach. A generated error surface was added to the DEM in each simulation and the probability of future inundation was calculated as the proportion of times a DEM cell was inundated from 1,000 simulations. Leon *et al*. (2014), however, only modeled one sea-level rise projection, and, therefore, did not incorporate the uncertainty of future sea-level rise. Furthermore, Leon *et al*. (2014) modeled a uniform storm surge height of 2.9-m for the entire study area. Storm surge heights typically vary along a coastline due to the offshore bathymetry and nearshore topography (Jelesnianski *et al*. 1992, McInnes *et al*. 2003).

The methods in Leon *et al*. (2014), and their limitations, informed the GIS framework for probabilistic modeling of future coastal flood zones in this study. Specifically, this study implemented a similar probabilistic approach as Leon *et al*. (2014) that incorporated DEM uncertainty, and also incorporated the uncertainties in the present-day 1% flood zone from storm surge and future sea-level rise projections.

Methodology

This study implemented a Monte Carlo approach to model the future 1% flood zone extent in Tottenville, NYC in a probabilistic, GIS framework. The future flood model incorporated the uncertainties in a topographic DEM, present-day 1% flood zone from storm surge, and future sea-level rise projections. A 500-member, future flood model ensemble was generated from random combinations of input data realizations within estimated uncertainty bounds. Open source software, including MB-System (Version 5.4.2220, Caress and Chayes 1996) and Python Version 2.7, was used to develop the future flood model and to derive spatiotemporal statistical products from the Monte

Carlo ensemble. The derived statistical products can inform coastal management policies by indicating the likelihood of the future 1% flood zone extent in Tottenville, NYC.

Study area

Tottenville is the southernmost neighborhood of Staten Island, NYC (Figure 1). The land-use in Tottenville is primarily residential, and the neighborhood is surrounded by water in three cardinal directions. The Arthur Kill is located to the west, and the Raritan Bay is located to the south and to the east of the neighborhood. Tottenville has a maximum elevation of ~30-m above the North American Vertical Datum 1988 (NAVD 88). Most of the neighborhood is currently protected from coastal flooding at these higher elevations, however, additional areas will likely become prone to future storm surge inundation enhanced by sea-level rise and be in the future 1% flood zone.

Digital elevation model (DEM)

Woolpert, Inc. collected topographic LIDAR between March 21–21 April 2014 for the U.S. Geological Survey (USGS) Coastal Marine and Geology Program (CMGP) Post-Sandy project (Woolpert 2014). The data set was collected to achieve a maximum nominal post spacing of LIDAR returns of 0.7-m, and 0.42-m horizontal accuracy at 95%

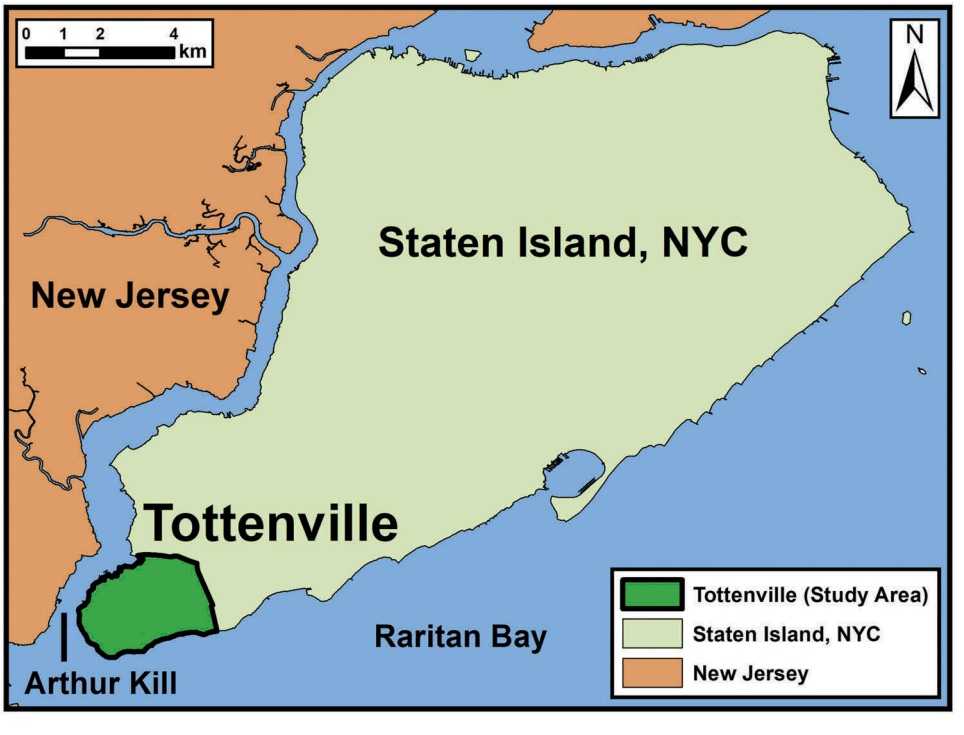

Figure 1. The Tottenville neighborhood of Staten Island, NYC is the study area to model future coastal flood zones.

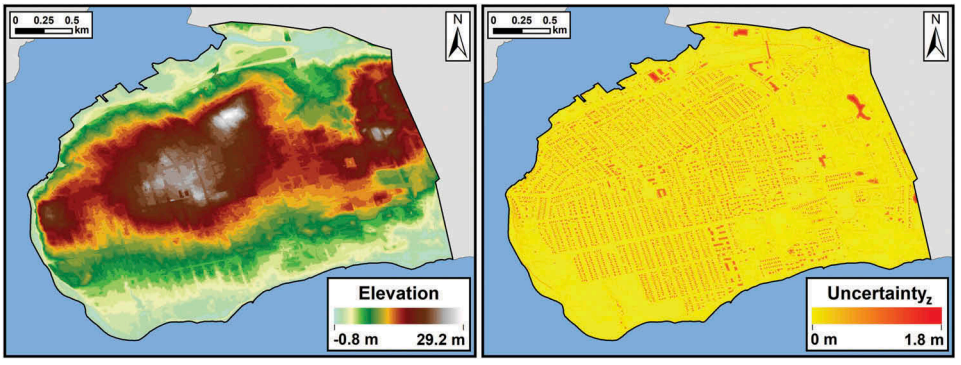

Figure 2. The DEM (Left Panel) and derived vertical uncertainty surface at one standard deviation (Right Panel). The largest uncertainties, and consequently, the largest differences between the DEM realizations in the future flood model, are located where there are large interpolation distances due to no LIDAR bare-earth returns, including inland bodies of water and within building footprints.

confidence (Woolpert 2014). The overall vertical accuracy for bare-earth LIDAR returns was 5.3-cm root mean square error ($RMSE_z$, Woolpert 2014).

A bare-earth, topographic DEM (Figure 2, Left Panel) was generated from the LIDAR bare-earth returns with spline interpolation from the open-source software tool, MB-System's 'mbgrid.' The generated DEM was referenced horizontally to the World Geodetic System 1984 (WGS 84) and vertically to NAVD 88. The DEM spatial resolution, $1/9^{th}$ arc-second (~3-m), followed the highest-resolution of the framework collaboratively developed by NOAA National Centers for Environmental Information (NCEI) and USGS (Eakins *et al*. 2015). Refer to Eakins and Taylor (2010) and Eakins and Grothe (2014) for additional details on NOAA NCEI coastal DEM generation and associated challenges.

An uncertainty surface that estimated potential DEM cell-level vertical errors at one standard deviation (Figure 2, Right Panel) was generated with the methods from Amante (2018b). The uncertainty surface represented contributions from the (1) measurement uncertainty provided in the LIDAR metadata (*i.e*., 5.3-cm $RMSE_z$) with an assumed non-biased, normal distribution, (2) number of measurements per DEM cell, (3) subcell measurement variance, and (4) interpolation uncertainty in cells unconstrained by measurements. In DEM cells with LIDAR bare-earth returns, the cell-level vertical uncertainty was calculated from a pooled standard deviation that incorporated the measurement uncertainty of 5.3-cm $RMSE_z$, and subcell measurement variance from the mean elevation of the DEM cell. The pooled standard deviation was divided by the square root of the number of measurements in the DEM cell to calculate the standard deviation of the mean, *i.e*., the standard error, to represent the DEM cell-level vertical uncertainty. There was additional uncertainty in interpolated DEM cells with no LIDAR bare-earth returns (*e.g*., water bodies and within building footprints), with larger distances from elevation measurements resulting in larger interpolation uncertainty (Amante and Eakins 2016, Amante 2018b). Refer to Amante (2018b) for additional details on the methods to estimate coastal DEM uncertainty at the individual cell-level.

Amante (2018b) created a DEM uncertainty surface that was spatially correlated with land cover and terrain slope. To confirm these results from Amante (2018b), this study

calculated the average cell-level uncertainty for land cover classes from the 2010 NYC Department of Parks and Recreation land cover raster (NYC Department of Parks and Recreation 2010). Furthermore, this study quantified the effect of both the land cover and terrain slope derived from the DEM (Figure 3) on the magnitude of the cell-level uncertainty with Spearman's rank correlation coefficients (Spearman 1904).

The two land cover classes with the largest, average cell-level uncertainty were the 'water' and 'building' classes due to few LIDAR bare-earth returns and interpolated DEM values in cells unconstrained by elevation measurements (Table 1). The two land cover classes with the smallest, average cell-level uncertainty were the 'road/railroad' and 'bare

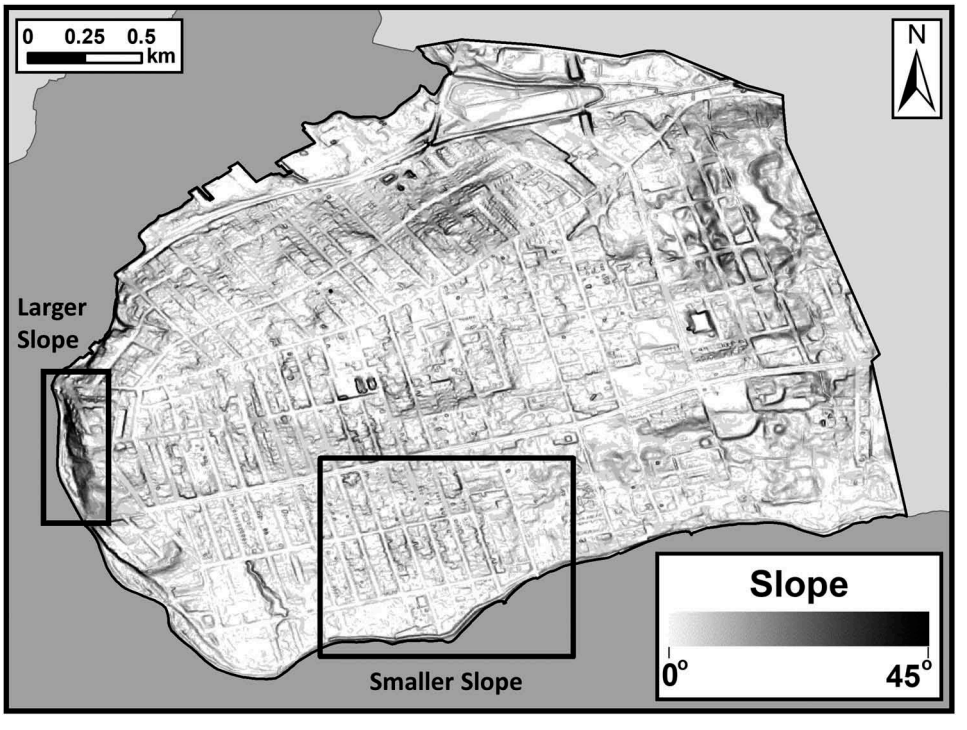

Figure 3. The terrain slope derived from the DEM. The slope varies within the study area, with larger terrain slope along the western coastline and smaller terrain slope along the southern coastline of the neighborhood.

Table 1. Effect of land cover and terrain slope on the magnitude of the DEM cell-level uncertainty. The number of DEM cells, *i.e.* sample size, for each of the four land cover classes was greater than 3,800, and all Spearman's rank correlation coefficients had p-values less than 0.001.

Land Cover Class	Avg. Cell-level Uncertainty: 1 St. Dev. (m)	Avg. Num. of Measurements per DEM Cell	Avg. Slope (degrees)	Spearman's Coefficient: Uncertainty and Num. of Measurements	Spearman's Coefficient: Uncertainty and Slope
Water	0.267	~ 4	1.586	−0.745	−0.649
Building	0.218	~ 2	2.628	−0.551	0.025
Bare Soil	0.031	~ 15	4.275	−0.176	0.671
Road/Railroad	0.028	~ 10	1.681	−0.501	0.339

soil' classes due to effective laser pulse penetration in open terrain, and consequently, many LIDAR bare-earth returns per DEM cell (Table 1).

The Spearman's rank correlation coefficients indicated a negative correlation between the magnitude of the DEM uncertainty and the number of measurements for these four land cover classes (Table 1), *i.e.*, more measurements per DEM cell resulted in smaller cell-level uncertainty, as expected per Amante (2018b). With the exception of the 'water' class, the terrain slope was positively correlated with the cell-level uncertainty (Table 1), as larger terrain slope resulted in larger subcell measurement variance, as expected per Amante (2018b). Topographic LIDAR systems typically do not produce bare-earth returns within water bodies. In such areas, DEM values were interpolated based on the elevations of bare-earth returns on the perimeters of these water bodies and produced relatively flat elevation surfaces. DEM uncertainty, therefore, was negatively correlated with terrain slope for the 'water' class because areas with the largest elevation uncertainty were in the center of water bodies due to large interpolation distances from the LIDAR bare-earth measurements, and these areas have small slope values. The DEM uncertainty was most positively correlated with terrain slope for the 'bare soil' class (Table 1), due to larger subcell measurement variance in steep, near-shore sand dunes.

This study generated DEM realizations for the future flood model using the DEM and derived cell-level uncertainty surface at one standard deviation. A normal, non-biased distribution was assumed, and the 'best-case' and 'worst-case' error realizations were created by multiplying the entire uncertainty surface at one standard deviation by 1.96 and −1.96 to represent the 95% confidence interval, respectively. The resulting error realizations were each added to the original DEM to create the 'best-case' and 'worst-case' DEM realizations, respectively. 498 additional, intermediate DEM realizations were then randomly generated using the derived uncertainty surface at one standard deviation and a mean of zero with the Numerical Python (NumPy) package function 'numpy.random.normal'. A 3 × 3 low-pass filter was applied to reduce the introduced noise and maintain the spatial autocorrelation of the terrain (Wechsler and Kroll 2006, Wechsler 2007), and each resulting error realization was added to the original DEM. The 500 generated DEM realizations, with a normal distribution, represented the DEM uncertainty incorporated in the future flood model.

Present-day storm surge

Two versions of the present-day FEMA 1% flood zones, the current, accepted 2007 FIRM, and the 2013 Preliminary FIRM, represented the 'best-case' and 'worst-case' scenarios of the present-day storm surge and wave heights in the future flood model, respectively. On 17 October 2016, FEMA announced the administration of the mayor of NYC, Bill de Blasio, won its appeal of the 2013 Preliminary FIRM, and FEMA agreed to revise the NYC FIRM (FEMA 2016). The appeal cited two primary sources of bias in the storm surge and offshore wave models that resulted in more inland areas within the 1% flood zone than warranted: (1) insufficient extratropical storm model validation and (2) misrepresentation of tidal effects for extratropical storms (Zarrilli 2015).

498 additional, intermediate present-day 1% flood zone realizations were randomly generated between the 2007 and 2013 FIRM 1% flood zone extents. Intermediate,

present-day total flood areas were randomly sampled between the total areas in the 1% flood zone for the 2007 and 2013 FIRMs with the python function 'numpy.random.uniform.' Next, initial water levels were estimated as the elevation values from the original DEM along the inland extent of the 2007 FIRM 1% flood zone. The initial water levels were iteratively raised by 0.01-m and the linear addition by expansion method was used to flood additional areas where the cumulative water levels were greater than the DEM values. Additional areas were flooded beyond the 2007 FIRM, but within the 2013 FIRM 1% flood zone, until the randomly sampled total flood area criteria was met. Generating intermediate present-day 1% flood zone realizations based on the DEM was more realistic than realizations based on arbitrary distances between the 2007 and 2013 FIRM 1% flood zone extents. Figure 4 illustrates the intermediate present-day 1% flood zone realizations between the 2007 and 2013 FIRMs.

Storm surge is typically a larger factor in coastal flooding than wave action for locations with wide and gently sloping continental shelves (Walsh *et al*. 2012), such as off the U.S. East Coast. Accordingly, this study refers to the initial water level heights in the future flood model derived from the 1% flood zone realizations simply as storm surge heights. The 500 generated present-day 1% flood zone realizations, with a uniform distribution, represented the present-day storm surge uncertainty incorporated in the future flood model.

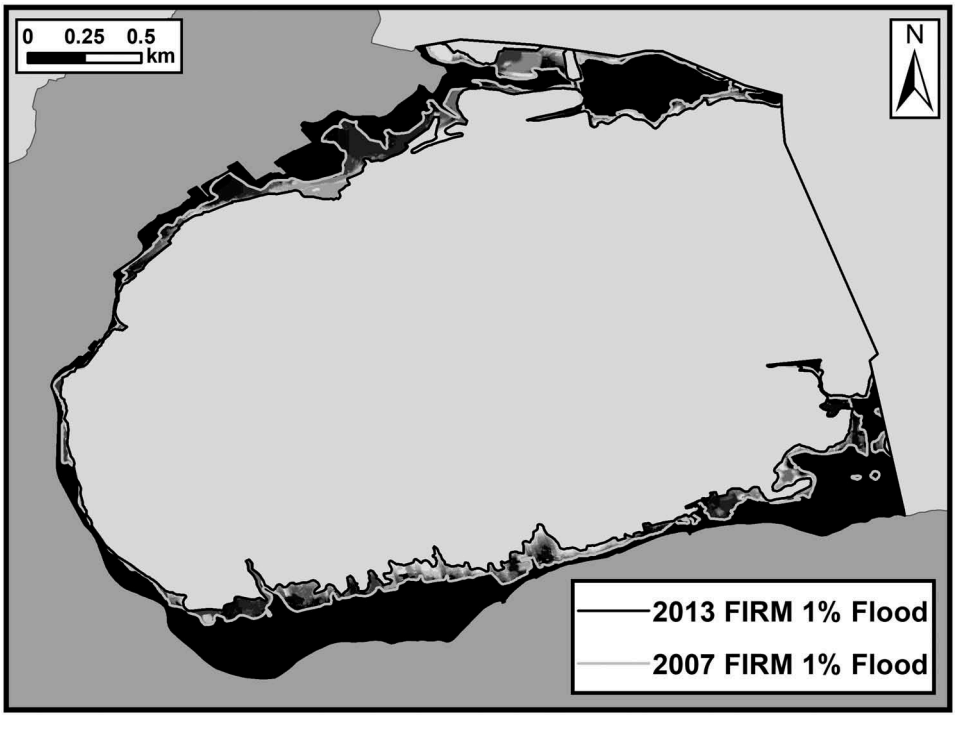

Figure 4. The present-day FEMA 1% flood zone represented by the 2007 FIRM and 2013 Preliminary FIRM. Intermediate, present-day 1% flood zone realizations were randomly generated between these two FIRMs based on the DEM; darker colors between the two FIRMs represent areas more likely to be in the present-day 1% flood zone realizations.

Sea-level rise

This study incorporated local sea-level rise projections from the NYC Panel on Climate Change (NPCC) 2015 report in the future flood model (Horton *et al*. 2015). The NPCC 2015 report aggregated individual components of sea-level rise to generate low (*i.e*., 10th percentile) and high (*i.e*., 90th percentile) sea-level rise estimates (Horton *et al*. 2015). The individual components included global thermal expansion, local changes in ocean height, loss of ice from Greenland and Antarctic ice sheets, loss of ice from glaciers and ice caps, gravitation, rotational, and elastic 'fingerprints' of ice loss, vertical land movements/glacial isostatic adjustments, and land-water storage (Horton *et al*. 2015). Refer to Table 2.2 in Horton *et al*. (2015) for the NPCC specific estimates of sea-level rise for the 2020s, 2050s, 2080s, and 2100.

The NPCC sea-level rise projections were referenced to a 2000–2004 baseline. This study modified the NPCC sea-level rise projections to be relative to 2014, which is the year of the LIDAR collection that generated the DEM. The relative sea-level trend from a nearby NOAA Tides and Current station (Sandy Hook, New Jersey, NOAA 2018) indicated a linear rate of 0.406-cm sea-level rise per year. Accordingly, the year 2002 was considered the middle of the baseline, and the NPCC low and high estimates were reduced by 4.872-cm to approximate the future sea-level rise projections relative to 2014. Two future sea-level rise projections were derived for each decade through 2100 from the NPCC low and high estimates with 2nd degree polynomials using the python function 'numpy.polyfit', to represent the 'best-case' and 'worst-case' scenarios, respectively. 498 additional, intermediate sea-level rise projections were then derived randomly between the low and high estimates with the python functions 'numpy.random.uniform' and 'numpy.polyfit' (Figure 5). The 500 generated sea-level rise projections, with a uniform distribution, represented the sea-level rise uncertainty incorporated in the future flood model.

Future flood model

The future flood model implemented the GIS-based, static linear addition by expansion method with Python Version 2.7, and, primarily, the NumPy and Scientific Python (SciPy) packages. First, initial storm surge heights were estimated as the elevation values from the original DEM along the inland extent of the randomly generated present-day 1% flood zone realization. A randomly generated sea-level rise projection was then added to these initial water heights and additional inundated areas were determined iteratively with array convolution and arithmetic functions from the SciPy and NumPy packages, respectively (Figure 6).

Starting at the inland extent of the randomly generated 1% flood zone realization, the water heights of the dry cells in the randomly generated DEM realization were calculated as the average water height of adjacent inundated cells. The dry cells then became inundated if their elevations were less than these calculated average water heights. This process was repeated until no new dry cells were inundated. The flood model recorded the year at which the calculated average water heights from the randomly generated present-day storm surge heights and future sea-level rise projection became greater

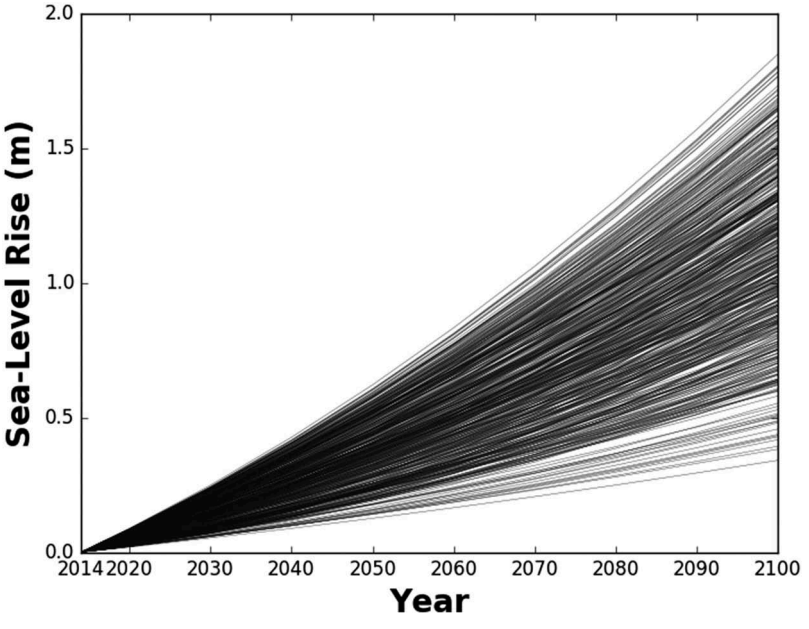

Figure 5. 500 randomly generated sea-level rise projections within the low and high estimates of sea-level rise in the NPCC 2015 report, relative to 2014. The differences in projected sea-level rise increases in future years due primarily to increasing uncertainty in the magnitude of ice sheet melt.

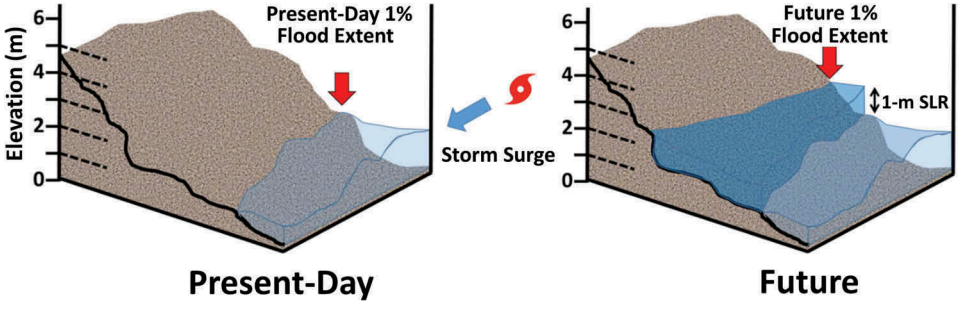

Figure 6. Illustrative schematic of the future flood model. The present-day 1% flood extent indicates the current coastal flood zone (Left Panel). The future 1% flood zone (Right Panel) is determined by adding a sea-level rise projection (*e.g.*, 1-m sea-level rise (SLR)) to the water heights estimated from the DEM values along the present-day 1% flood extent. Additional areas are flooded where the cumulative water heights are greater than the DEM values.

than each DEM realization cell. An 8-neighbor water connectivity algorithm defined the cell adjacency and was implemented to avoid incorrectly inundating inland local depressions not connected to the present-day or modeled future ocean. The 8-neighbor algorithm was implemented to model the 'worst-case' scenario of water connectivity, as the 4-neighbor algorithm is a conservative estimate of water connectivity and can potentially result in less inundation due to terrain barriers of water flow.

Monte Carlo simulations

This study implemented a Monte Carlo approach to incorporate random combinations of input data realizations and create a 500-member, future flood model ensemble (*e.g.*, Heuvelink *et al*. 1999, Cooper and Chen 2013, Leon *et al*. 2014, Schmid *et al*. 2014, West *et al*. 2018). Each of the 498 intermediate simulations consisted of randomly generated input data realizations within the minimum and maximum DEM, sea-level rise, and storm surge values in Table 2. The year inundated for each DEM cell was recorded in each simulation, resulting in a distribution of years inundated for each cell based on the random combinations of the input data realizations. Spatiotemporal statistical products were then generated from the cell-level distributions of the year inundated to indicate the likelihood of the future 1% flood zone extent in Tottenville, NYC. The effect of the input data realizations on the modeled total area in the future 1% flood zone was also quantified with Spearman's rank correlation coefficients (Spearman 1904).

Interactive web map to host statistical products

An interactive web map, UncertainSeas.com, visualizes the spatiotemporal statistical products that depict the future 1% flood zone in Tottenville, NYC. One statistical product depicts the annual probability of the future 1% flood zone for each decade through 2100. The annual probability was calculated for each DEM cell as the number of times the cell was flooded by the specified year out of the 500-member ensemble, and larger probabilities indicate areas more likely to be located within the future 1% flood zone.

Another statistical product, alternatively, depicts the year in which each DEM cell exceeds a given annual probability of being in the future 1% flood zone. This probability exceedance year statistical product can be especially useful for local coastal management policies because communities can have much different risk tolerances to coastal flooding. This statistical product can indicate *when* a community should implement policies to reduce the vulnerability of an area to flooding, depending on their risk tolerance. For example, 'Community Z' will implement policies to reduce the vulnerability of an area to coastal flooding only when there is a 95% chance of the area being in the future 1% flood zone (*i.e.*, they have a high-risk tolerance). Conversely, 'Community Y' is risk-averse and will implement policies to reduce the vulnerability of the same area when there is a 5% chance of the area being in the future 1% flood zone. These different risk tolerances would result in 'Community Y' implementing policies to reduce the vulnerability of an area to coastal flooding earlier than 'Community Z.'

Table 2. Input data in the Monte Carlo simulations, and their 'best-case' and 'worst-case' values that delineate the future minimum and maximum flood zone extents, respectively. 498 additional, random combinations of each input data source realization within the minimum and maximum flood extent values generated the 500-member ensemble. The DEM realizations were randomly sampled from a normal distribution, whereas the sea-level rise and storm surge realizations were randomly sampled from a uniform distribution between the minimum and maximum values in this table.

Input data	Data source	Minimum flood extent	Maximum flood extent
DEM	USGS	DEM + (1.96 * Uncertainty Surface)	DEM – (1.96 * Uncertainty Surface)
Sea-level Rise	NPCC	Low Sea-level Rise Estimate	High Sea-level Rise Estimate
Storm Surge	FEMA	2007 FIRM 1% Flood Extent	2013 Preliminary FIRM 1% Flood Extent

Results

The future flood model for Tottenville, NYC incorporated multiple input data uncertainties in a GIS, probabilistic framework. Figure 7 indicates the Tottenville land area in the future 1% flood zone through the year 2100 for each of the 500 members of the Monte Carlo ensemble. The area in the future 1% flood zone varies between approximately 1.1 to 1.8 km^2 by the year 2100 and corresponds to the input data values that produce the minimum and maximum flood extents in Table 2, respectively.

Figure 8 illustrates the effect of the input data realizations on the total area in the future 1% flood zone for every decade through 2100. The storm surge realizations have the largest correlation coefficients with the total area in the future flood zone between 2020–2050. After 2050, the sea-level rise realizations have larger correlation coefficients with the total area in the future 1% flood zone due to larger uncertainty in sea-level rise projections in these more distant decades. The correlation coefficients between the storm surge and sea-level rise realizations and the total area in the future 1% flood zone all have p-values less than 0.001 for each decade through 2100, except for the sea-level rise realizations for the year 2020. The DEM realizations have much smaller correlation coefficients with the total area in the future 1% flood zone and the p-values are greater than 0.37 for each decade through 2100.

Spatiotemporal statistical products derived from the Monte Carlo ensemble hosted on the interactive web map, UncertainSeas.com, address limitations of the non-spatial metric of the total land area in the future 1% flood zone. These statistical products indicate areas with high elevations in the center of the neighborhood should remain protected from coastal inundation into the distant future (*i.e.*, 2100), even with the 'worst-case' DEM, sea-level rise, and storm surge realizations that produced the maximum flood extent in Table 2.

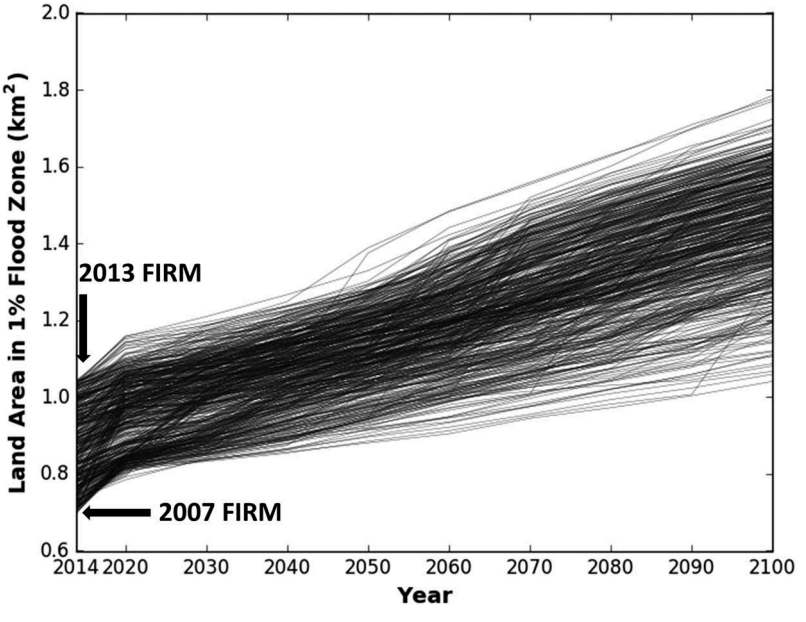

Figure 7. The modeled land area in the future 1% flood zone in Tottenville for each of the 500 members of the Monte Carlo ensemble.

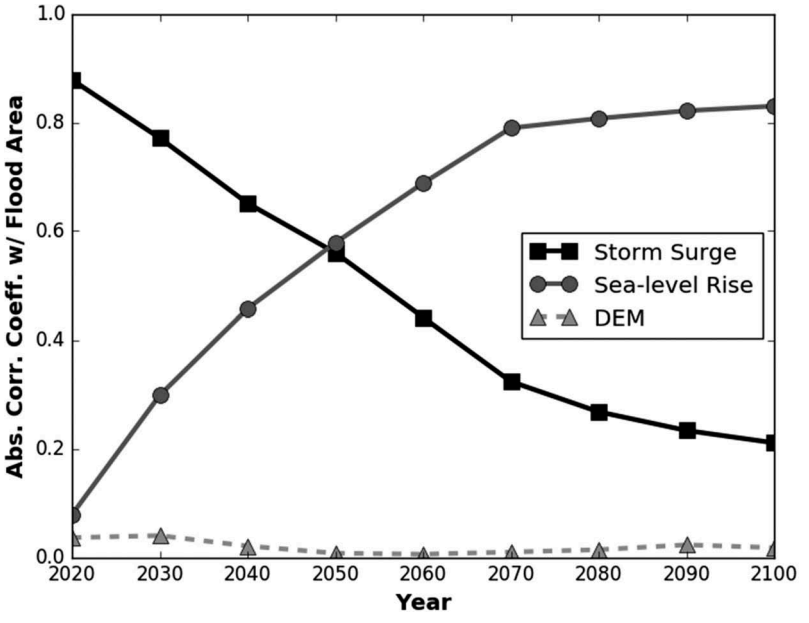

Figure 8. The effect of the input data realizations on the total land area in the future 1% flood zone. The storm surge realizations have the largest correlation coefficients with the total land area in the future flood zone until 2050. After 2050, the sea-level rise realizations have the largest correlation coefficients with the total land area in the future 1% flood zone.

Conversely, low-lying areas, such as along the northern and southern coasts of Tottenville, are already prone to coastal inundation, and the likelihood of adjacent areas being in the 1% flood zone increases in future decades, even with the 'best-case' realizations of the input data in Table 2.

Probability of future flood zone

Figure 9 visualizes the annual probability of coastal locations in Tottenville being in the future 1% flood zone for the years 2020, 2060, and 2100, respectively. The inland extent of the future 1% flood zone remains relatively constant over time due to high elevations in the center of Tottenville that approach ~30-m above NAVD 88, however, the likelihood of many coastal locations being in the future 1% flood zone increases over time due to projected sea-level rise.

The area in the box shown in Figure 9 has larger uncertainty in the future 1% flood zone extent due to low-lying elevations with smaller terrain slope. The probability of the future 1% flood zone in the year 2100 in this highlighted area is shown in the left side of Figure 10. The horizontal band of probabilities that range from 0 to 100% in the left side of Figure 10 illustrates the uncertainty of the future flood zone extent. The right side of Figure 10 indicates the annual probability of being in the future 1% flood zone for three locations (A, B, and C) through 2100. The annual probability of being in the future flood zone increases over time for these three locations due to projected increases in sea-level rise.

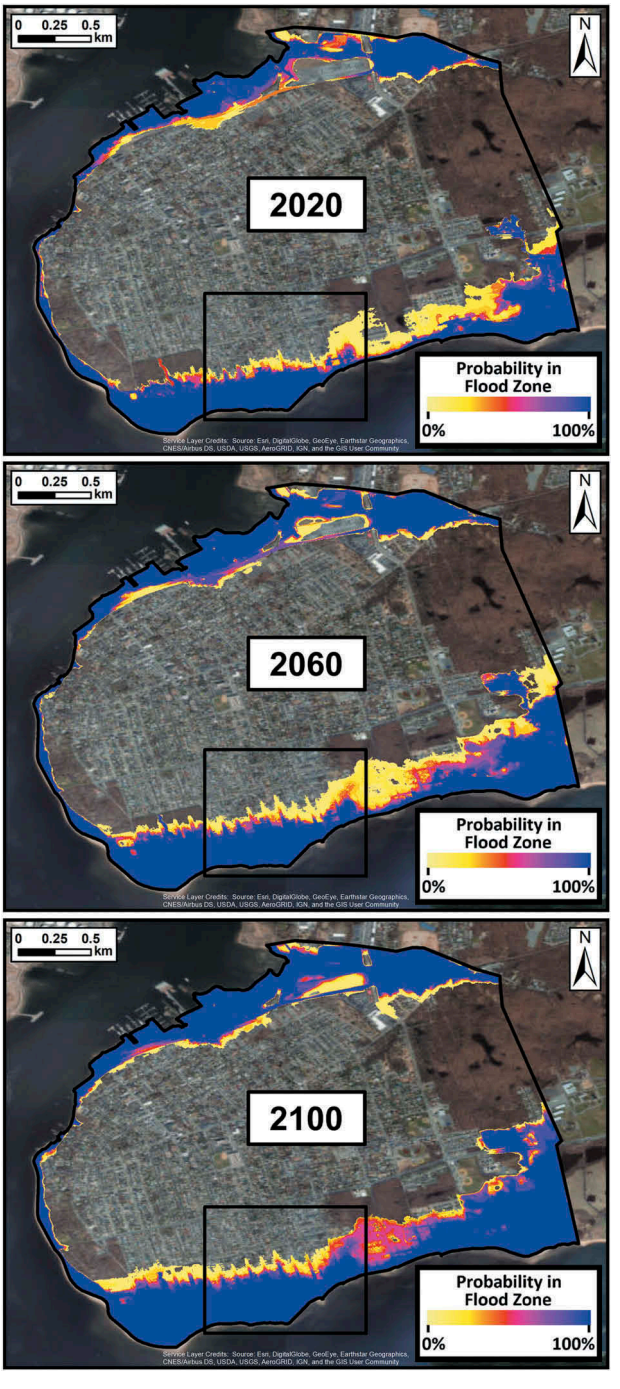

Figure 9. The annual probability of areas being in the future 1% flood zone for the years 2020, 2060, and 2100. The box in each panel highlights the area of Tottenville with larger uncertainty in the future flood zone extent, and this area is shown in greater detail in Figure 10.

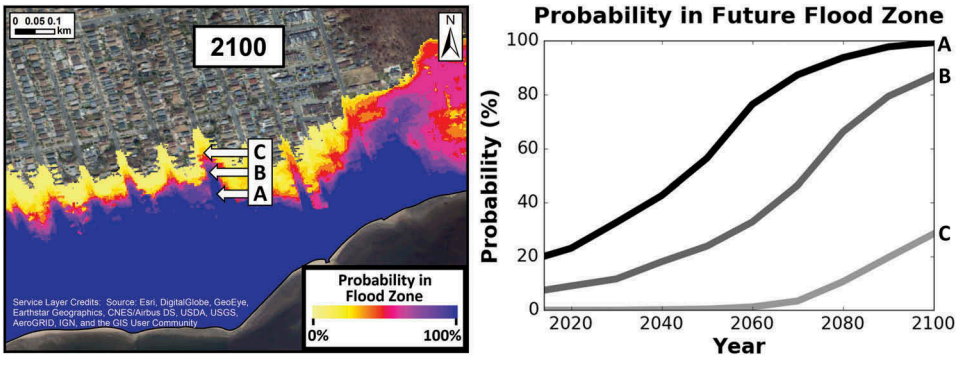

Figure 10. The annual probability of areas being in the future 1% flood zone in the year 2100 is highlighted for a portion of the study area (Left Panel). The band of probabilities that range from 0 to 100% illustrates the horizontal uncertainty of the future flood zone extent in this portion of the study area. The line graph (Right Panel) indicates the annual probability of being in the future flood zone increases over time for all three locations (A, B, and C), due to projected sea-level rise.

Probability exceedance year

Figure 11 illustrates the year in which each DEM cell in this same highlighted area exceeds the 95%, 50%, and 5% annual probability of being in the future 1% flood zone. These different highlighted probabilities correspond to potential differences in a community's risk tolerance to coastal flooding. For example, the highest risk tolerance to flooding, the 95% probability, results in most areas not being in the future flood 1% zone until after 2100. Conversely, the lowest risk tolerance, the 5% probability, results in many of these same areas being in the 1% flood zone in the near future. Temporal information on the expansion of future flood zones is critical for coastal management policies, and the individual community's risk tolerance determines when to implement policies to reduce the vulnerability of an area to coastal flooding.

Uncertainseas.com

The interactive web map, UncertainSeas.com, visualizes the spatiotemporal statistical products and provides a suite of decision-making tools to inform coastal management policies in Tottenville (Figure 12). The web map hosts the statistical products that indicate the DEM cell-level annual probability of being in the future 1% flood zone for every decade from 2020 through 2100. The web map also hosts the novel statistical products that spatially depict the year at which various annual probabilities of being in the future 1% flood zone are exceeded in Tottenville (*i.e.*, exceeds the 5%, 25%, 50%, 75%, and 95% probability).

Discussion

Studies that model future coastal inundation typically do not incorporate all major sources of input data uncertainties, *i.e.*, the storm surge, sea-level rise, and DEM uncertainties. The probabilistic framework in this study incorporates these input data

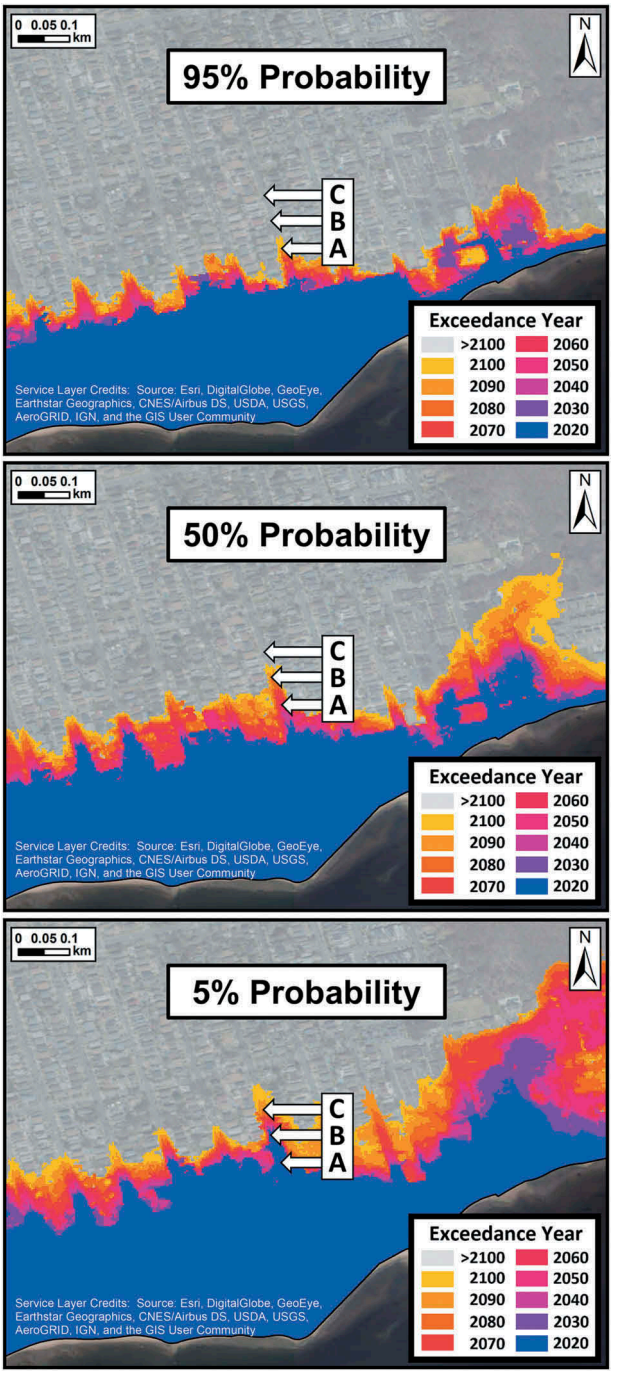

Figure 11. Example of the annual probability exceedance year data product for the same portion of the study area shown in Figure 10. The maps depict the year at which each DEM cell exceeds a given annual probability of being in the future 1% flood zone. Three probabilities, 95%, 50%, and 5%, are shown to represent potential differences in a community's risk tolerance to future coastal flooding.

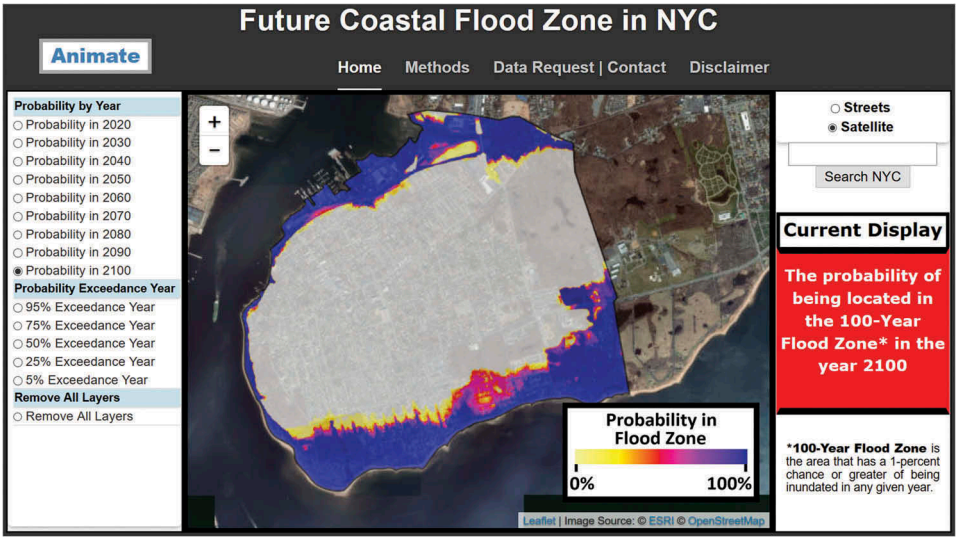

Figure 12. Screenshot of the interactive web map, UncertainSeas.com, that hosts the spatiotemporal statistical products indicating the future 1% flood zone in Tottenville, NYC.

uncertainties and accounts for possible non-linear interactions in modeling the future 1% flood zone extent in Tottenville, NYC.

The spatiotemporal statistical products hosted on UncertainSeas.com have many advantages over standard reports, paper maps, and the figures in this manuscript in depicting the future 1% flood zone and its uncertainty in Tottenville. The web map can facilitate interactive planning for a specific location, house, business, or infrastructure over time as coastal flood zones in Tottenville expand in the future due to projected sea-level rise. However, web map-users must remain aware of the limitations of the generated spatiotemporal statistical products due to inherent uncertainty in geospatial data, including the estimated storm surge, sea-level rise, and DEM uncertainties, and their incorporation in the future flood model.

The probability exceedance year statistical product hosted on UncertainSeas.com can be especially useful for individualized coastal management policies. This statistical product enables a uniform probability threshold to be established based on the individual community's risk tolerance, and the year at which areas are prone to flooding based on that probability threshold are depicted. The temporal information is important for coastal management policies, and the high temporal resolution of the statistical products, *i.e.*, every decade, also advances previous studies, which often model only one year in the distant future, such as the year 2100.

Future flood zone in Tottenville, NYC

Spatiotemporal statistical products generated from the Monte Carlo ensemble indicate the future 1% flood zone extent and its uncertainty in Tottenville, NYC. One statistical product illustrates the annual probability of being in the future 1% flood zone for each decade through 2100. This annual probability is calculated as the proportion of times

DEM cells are flooded by the given year from the 500-member ensemble and should not be confused with the traditional, cumulative probability of flooding. For example, the traditional, cumulative probability of flooding indicates a building located in the current 1% flood zone has a greater than 26% chance of being flooded by at least one 1% magnitude flood over the course of the standard 30-year mortgage (Pielke, Jr. 1999, Burby 2001). This larger, cumulative probability of flooding further emphasizes the need to protect areas of Tottenville immediately, such as along the northern and southern coasts of the neighborhood.

Effect of input data uncertainties

Figure 8 indicates that the storm surge realizations have the largest correlation coefficients with the total area in the future flood zone in the coming decades (*i.e.*, 2020–2050). This is not surprising, given the accepted legal challenge to the 2013 Preliminary FIRM, and the large, present-day storm surge uncertainty illustrated in Figure 4. Furthermore, there is little consensus on how storms in NYC will change in future climates (Orton *et al*. 2015, Sweet *et al*. 2017). There is medium confidence in a projected increase in the intensity of hurricanes in the North Atlantic (Sweet *et al*. 2017). However, there is low confidence in the projected increase in frequency of intense Atlantic hurricanes, and the associated amplification of flooding could be offset or amplified by changes in overall storm frequency or tracks (Sweet *et al*. 2017). Future sea-level rise can also reduce the rate at which low-lying areas drain, increasing the likelihood of flooding from rainfall (Titus *et al*. 1987), which was not incorporated in this study. Potential changes in future storm climatology and additional flooding from rainfall provide justification for incorporating the 'overly pessimistic' 2013 Preliminary FIRM in the future flood model.

The 2007 and 2013 FIRMs have differences in the flooded elevations of greater than 1-m in the same, general vicinity along the southern coastline of Tottenville. The differences between sea-level rise projections in the near-future and the DEM realizations are much smaller than this 1-m difference in the storm surge height representations. For example, in the year 2025, the difference between the low and the high sea-level rise estimates from the NPCC 2015 report is ~0.2-m (Horton *et al*. 2015). Differences in DEM realizations in Tottenville are also relatively small, as the average cell-level uncertainty at one standard deviation is only ~0.05-m due to modern, LIDAR technology (Amante 2018a). Incorporating DEM uncertainty in flood models is more important for coastal communities with topographic elevations mapped with older, less accurate technologies, such as with Shuttle Radar Topography Mission (SRTM) interferometric radar data (Rabus *et al*. 2003). For example, SRTM elevation products have absolute height errors of 5.6-m at the 90% confidence level for the continent of Africa (Rodriguez *et al*. 2005). Differences in DEM realizations would likely have a larger effect on the modeled future flood zone for coastal communities mapped with these older, less accurate technologies.

The effect of the input data realizations on the modeled total area in the future 1% flood zone illustrated in Figure 8 also changes over time. The sea-level rise uncertainty increases over time due to increasing uncertainty in the magnitude of ice sheet melt (Horton *et al*. 2015), and, consequently, the sea-level rise realizations have the largest correlation coefficients with the total area in the future 1% flood zone after 2050. It should be noted sea-level rise uncertainty and DEM uncertainty are intertwined, as the

sea-level rise estimates in the NPCC 2015 report consider future, local land subsidence and its uncertainty (Horton *et al*. 2015).

The generated spatiotemporal statistical products illustrate the uncertainty in the future flood zone extent that results from the uncertainties in the input data sources and from the terrain itself. Figure 9 indicates there are portions of Tottenville with larger horizontal bands of uncertainty in the future flood zone extent. This occurs in low-lying areas with smaller terrain slope, such as the area highlighted along the southern coast of Tottenville in Figures 3, 9, 10, and 11. In such areas, small changes in the modeled land and water heights within the estimated uncertainties of the data sources results in larger uncertainty in the future flood zone extent. Conversely, areas with larger terrain slope, such as along the western coast of Tottenville highlighted in Figure 3, have a much narrower band of horizontal uncertainty in the future flood zone extent. These results support previous findings on the impact of terrain slope on the horizontal uncertainty of the future flood zone extent (Gesch 2013, West *et al*. 2018). Incorporating input data uncertainties in coastal flood models is especially important for communities with heterogeneous terrain, such as Tottenville, which can result in low-lying areas with smaller terrain slope having greater uncertainty in the future flood zone extent.

Limitations and future research

The estimation and incorporation of the input data uncertainties in the coastal flood model can be improved in future research. The DEM cell-level uncertainty estimation is limited by the incorporated measurement uncertainty from the LIDAR dataset's metadata. This uniform measurement uncertainty of 5.3-cm $RMSE_z$ should be refined in future research using accurate ground control measurements because LIDAR measurement uncertainty is typically correlated with land cover and terrain (Su and Bork 2006, Bater and Coops 2009, Coveney and Fotheringham 2011, Spaete *et al*. 2011, Leon *et al*. 2014, Goulden *et al*. 2016, West *et al*. 2018). This study did, however, implement methods from Amante (2018b) that partially incorporate land cover and terrain effects on the magnitude of DEM cell-level uncertainty. These methods consider the number of measurements per DEM cell and the subcell measurement variance, resulting in a spatially-varying estimate of DEM cell-level uncertainty that is correlated with land cover and terrain slope, respectively (Table 1). Accurate ground control elevation measurements are also needed to identify any systematic, vertical errors in the DEM, which were not rigorously quantified in this study, but could cause differences in the modeled future coastal flood zone. Future morphologic changes, such as coastal erosion or accretion, were also not incorporated in the estimated DEM uncertainty. Additional components of DEM uncertainty are difficult, if not impossible to incorporate, including future drainage modifications (*e.g*., canals, ditches, culverts), and engineered barriers (*e.g*., levees, seawalls, flood gates, Gesch 2013).

The effect of the DEM spatial resolution on the modeled future flood zone was also not evaluated. The DEM spatial resolution must resolve important terrain features, such as channels or levees, which can enhance or impede the flow of water, respectively, by considering the Nyquist-Shannon sampling theorem. The Nyquist-Shannon sampling theorem states that terrain features must have dimensions at least twice the spatial resolution to be resolved by the DEM (Nyquist 1928, Shannon 1949, McBratney *et al*. 2003, Hengl 2006). Previous research indicates the modeled flood area generally

increases with coarser-resolution DEMs (*e.g.*, Saksena and Merwade 2015, Hsu *et al.* 2016), which is a manifestation of the scale effect of the modifiable areal unit problem (Openshaw 1977, 1983, Fotheringham and Wong 1991). DEMs with finer spatial resolutions than the 1/9th arc-second (~3-m) DEM in this study that are supported by the LIDAR dataset's post spacing of 0.7-m could be incorporated in future research to investigate the sensitivity of the modeled future flood zone to the DEM spatial resolution.

Another avenue of future research is to compare DEM realizations created using the different methods described in Wechsler (2007), including various spatial moving averages, pixel swapping, spatial autoregressive models, and sequential Gaussian simulation, and determine the sensitivity of the future flood model to these different DEM realizations. These future research endeavors to improve the estimation and incorporation of DEM uncertainty in coastal flood models should provide greater benefits to communities with topographic elevations mapped with older, less accurate technologies than topographic LIDAR.

GIS-based, static methods of modeling future storm surge inundation enhanced by sea-level rise typically use only a topographic DEM. Dynamic methods directly use a bathymetric DEM in the hydrodynamic storm surge models, and Amante (2018b) indicates the vertical uncertainty of offshore bathymetry can be much larger than the uncertainty of nearshore topography. The depth and shape of the seafloor can influence storm surge heights, and relatively wide and shallow continental shelves can amplify storm surge (McInnes *et al.* 2003, Walsh *et al.* 2012). The bathymetric uncertainty is often not incorporated in hydrodynamic storm surge models due to computational expense, and, therefore, this unincorporated bathymetric uncertainty provides further justification for using the 2013 Preliminary FIRM to represent additional storm surge uncertainty. Future research should model future flood zones with dynamic methods that use bathymetric DEMs directly to validate the GIS-based, static methodology implemented in this study. Future research should also investigate optimal mesh node locations for storm surge models based on the vertical uncertainty and horizontal precision of the underlying DEM (Amante 2018a), and the implications of storm surge mesh node locations in comparisons between dynamic and static methods of modeling future coastal flood zones.

This study focused on modeling the future 1% flood zone in Tottenville. Future research should also identify areas most vulnerable to both the physical hazard of future coastal flooding, as well as the social vulnerability to coastal flooding (*e.g.*, the SOcial Vulnerability Index (SOVI), Cutter *et al.* 2003). Important social factors to consider include the community's experience with coastal flooding, and the community's ability to respond to, cope with, recover from, and adapt to coastal flooding, which is influenced by the community's economic, demographic, and housing characteristics (Cutter *et al.* 2003). The social data uncertainties should also be incorporated in a similar probabilistic framework to model the areas and people of Tottenville that are most vulnerable to future coastal flooding and to quantify its uncertainty.

One large source of uncertainty that is difficult to quantify is a community's potential response to expanding flood zones, such as by engineering flood mitigation structures or with planned retreats from coastlines (Fleming 2018, Lempert 2018). An important

factor in a community's potential response is the perceived loss of culture and identity associated with unique cultural heritage sites and a sense of place (Lempert 2018). Collaborations between physical and social scientists are needed to incorporate all these sources of uncertainty in both physical and social models and to determine the overall vulnerability of communities to future coastal flooding.

Conclusions

This study implemented a Monte Carlo approach to model the future 1% flood zone extent in Tottenville, NYC in a probabilistic, GIS framework. The future flood model incorporated the uncertainties in a topographic DEM, present-day 1% flood zone from storm surge, and future sea-level rise projections. Generated spatiotemporal statistical products from the 500-member Monte Carlo ensemble indicate the future 1% flood zone extent and its uncertainty in Tottenville.

The spatiotemporal statistical products indicate areas with high elevations in the center of the neighborhood should remain protected from coastal inundation into the distant future (*i.e.*, 2100). Conversely, low-lying areas, such as along the northern and southern coasts of Tottenville, are already prone to coastal inundation, and the likelihood of being in the 1% flood zone increases in adjacent areas in future decades. The spatiotemporal statistical products also indicate the uncertainty in the future flood zone extent that results from the input data uncertainties and from the terrain itself. Small changes in the modeled land and water heights within the estimated uncertainties of the data sources result in larger uncertainty in the future flood zone extent in low-lying areas with smaller terrain slope.

An interactive web map, UncertainSeas.com, visualizes the likelihood of the future expansion of the 1% flood zone in Tottenville. The spatiotemporal statistical products hosted on the web map, combined with additional information on social vulnerability, can inform coastal management policies to reduce the overall vulnerability of the people, property and economy of Tottenville, NYC to future coastal inundation.

Acknowledgments

This research was part of my doctoral dissertation at the University of Colorado Boulder. I thank Waleed Abdalati, Barbara Buttenfield, Stefan Leyk, Seth Spielman, and Weiqing Han for their guidance throughout my doctoral studies. I also thank many at NOAA NCEI for their support, and the three anonymous reviewers and journal editor for their valuable feedback that significantly improved the quality of the manuscript.

Disclosure statement

No potential conflict of interest was reported by the author.

Notes on contributor

Christopher J. Amante is a Geospatial Research Scientist at the National Oceanic and Atmospheric Administration (NOAA) National Centers for Environmental Information (NCEI) through the Cooperative Institute for Research in Environmental Sciences (CIRES) at the University of Colorado Boulder.

ORCID

Christopher J. Amante http://orcid.org/0000-0001-8306-5552

References

Albert, S., *et al*. 2013. Cost-effective methods for accurate determination of sea level rise vulnerability: a Solomon Islands example. *Weather, Climate, and Society*, 5 (4), 285–292. doi:10.1175/WCAS-D-13-00010.1

Algeo, L. and Mahoney, T., 2011. FEMA's update process for coastal surge and wave analysis for flood insurance rate maps. *Solutions to Coastal Disasters*, 2011, 569–580.

Almeida, L.P., *et al*. 2019. Deriving high spatial-resolution coastal topography from sub-meter satellite stereo imagery. *Remote Sensing*, 11 (5), 590. doi:10.3390/rs11050590

Amante, C.J., 2018a. Consideration of elevation uncertainty in coastal flood models. Thesis (PhD). University of Colorado Boulder.

Amante, C.J., 2018b. Estimating coastal digital elevation model uncertainty. *Journal of Coastal Research*, 34 (6), 1382–1397. doi:10.2112/JCOASTRES-D-17-00211.1

Amante, C.J. and Eakins, B.W., 2016. Accuracy of interpolated bathymetry in digital elevation models. *In*: J.C. Brock, *et al*., eds. *Advances in topobathymetric mapping, models, and applications*. *Journal of Coastal Research*, Special Issue No. 76. Coconut Creek, Fl, 123–133, ISSN 0749-0208. doi:10.2112/SI76-011

Atkinson, J., *et al*. 2013. Sea level rise effects on storm surge and nearshore waves on the Texas coast: influence of landscape and storm characteristics. *Journal of Waterway, Port, Coastal, and Ocean Engineering*, 139 (2), 98–117. doi:10.1061/(ASCE)WW.1943-5460.0000187

Barnston, A.G. and Livezey, R.E., 1987. Classification, seasonality and persistence of low-frequency atmospheric circulation patterns. *Monthly Weather Review*, 115 (6), 1083–1126. doi:10.1175/1520-0493(1987)115<1083:CSAPOL>2.0.CO;2

Bater, C.W. and Coops, N.C., 2009. Evaluating error associated with lidar-derived DEM interpolation. *Computer Geosciences*, 35 (2), 289–300. doi:10.1016/j.cageo.2008.09.001

Blake, E.S., *et al*. 2013. Tropical cyclone report: Hurricane Sandy. *National Hurricane Center.*, 12, 1–10.

Burby, R.J., 2001. Flood insurance and floodplain management: the US experience. *Environmental Hazards*, 3 (3–4), 111–122. doi:10.3763/ehaz.2001.0310

Caress, D.W. and Chayes, D.N., 1996. Improved processing of hydrosweep DS multibeam data on the R/V Maurice Ewing. *Marine Geophysical Research*, 18 (6), 631–650. doi:10.1007/BF00313878

Cazenave, A. and Nerem, R.S., 2004. Present-day sea level change: observations and causes. *Reviews of Geophysics*, 42, 3. doi:10.1029/2003RG000139

Church, J.A., 2013. Sea Level Change. *In*: T.F. Stocker, *et al*., eds. *Climate change 2013: the physical science basis. Contribution of working group I to the fifth assessment report of the intergovernmental panel on climate change*. Cambridge, UK: Cambridge University Press, 1137–1216. doi:10.1017/CBO9781107415324.026

Cooper, H.M. and Chen, Q., 2013. Incorporating uncertainty of future sea-level rise estimates into vulnerability assessment: a case study in Kahului, Maui. *Climatic Change*, 121 (4), 635–647. doi:10.1007/s10584-013-0987-x

Coveney, S. and Fotheringham, A.S., 2011. The impact of DEM data source on prediction of flooding and erosion risk due to sea-level rise. *International Journal of Geographical Information Science*, 25 (7), 1191–1211. doi:10.1080/13658816.2010.545064

Cowell, P.J., *et al*., 2006. Management of uncertainty in predicting climate-change impacts on beaches. *Journal of Coastal Research*, 232–245. doi:10.2112/05A-0018.1

Cutter, S.L., *et al*., 2003. Social vulnerability to environmental hazards. *Social Science Quarterly*, 84, 242–261. doi:10.1111/1540-6237.8402002

Ding, Y., *et al*., 2013. Impact assessment of sea-level rise and hazardous storms on coasts and estuaries using integrated processes model. *Ocean Engineering*, 71, 74–95. doi:10.1016/j.oceaneng.2013.01.015

Eakins, B.W., *et al*., 2015. A framework for a seamless depiction of merged bathymetry and topography along U.S. coasts. *Proc. U.S. Hydro. Conf*., National Harbor, MD, 16–19 March 2015.

Eakins, B.W. and Grothe, P.R., 2014. Challenges in building coastal digital elevation models. *Journal of Coastal Research*, 30 (5), 942–953. doi:10.2112/JCOASTRES-D-13-00192.1

Eakins, B.W. and Taylor, L.A., 2010. Seamlessly integrating bathymetric and topographic data to support tsunami modeling and forecasting efforts. *In*: J. Bremen, ed. *Ocean globe*. Redlands, CA: ESRI Press Academic, 37–56.

FEMA, 2014. *Region II coastal storm surge study: overview*. Washington, DC: Risk Assessment, Mapping, and Planning Partners.

FEMA, 2016. Mayor De Blasio and FEMA Announce Plan to Revise NYC's Flood Maps. https://www.fema.gov/news-release/2016/10/17/mayor-de-blasio-and-fema-announce-plan-revise-nycs-flood-maps. Accessed 28 March 2018.

Fleming, E., 2018. Coastal effects. *In*: D.R. Reidmiller, *et al*., eds. *Impacts, risks, and adaptation in the United States: fourth national climate assessment, volume II*. Washington, DC, USA: U.S. Global Change Research Program, 322–352. doi:10.7930/NCA4.2018.CH8

Fotheringham, A.S. and Wong, D.W., 1991. The modifiable areal unit problem in multivariate statistical analysis. *Environment and Planning A*, 23 (7), 1025–1044. doi:10.1068/a231025

Frazier, T.G., *et al*. 2010. Influence of potential sea level rise on societal vulnerability to hurricane storm-surge hazards, Sarasota County, Florida. *Applied Geography*, 30 (4), 490–505. doi:10.1016/j.apgeog.2010.05.005

Gesch, D.B., 2009. Analysis of lidar elevation data for improved identification and delineation of lands vulnerable to sea-level rise. In:J.C. Brock and S.J. Purkis, eds. *Coastal applications of airborne lidar remote sensing*. Journal of Coastal Research, Special Issue No. 53. Coconut Creek, FL, 49–58, ISSN 0749-0208. doi:10.2112/SI53-006.1.

Gesch, D.B., 2012. Elevation uncertainty in coastal inundation hazard assessments. *In*: S. Cheval, ed. *Natural disasters*. Rijeka, Croatia: InTech, 121–140.

Gesch, D.B., 2013. Consideration of vertical uncertainty in elevation-based sea-level rise assessments: Mobile Bay, Alabama case study. *Journal of Coastal Research*, 63, 197–210. doi:10.2112/SI63-016.1

Goulden, T., *et al*., 2016. Sensitivity of DEM, slope, aspect and watershed attributes to LiDAR measurement uncertainty. *Remote Sensing of Environment*, 179, 23–35. doi:10.1016/j.rse.2016.03.005

Han, W., *et al*. 2017. Spatial patterns of sea level variability associated with natural internal climate modes. *Surveys in Geophysics*, 38 (1), 217–250. doi:10.1007/s10712-016-9386-y

Hare, R., *et al*. 2011. Modeling bathymetric uncertainty. *International Hydrographic Review*, 6, 31–42.

Hengl, T., 2006. Finding the right pixel size. *Computers & Geosciences*, 32 (9), 1283–1298. doi:10.1016/j.cageo.2005.11.008

Heuvelink, G.B.M., *et al*., 1999. Propagation of error in spatial modelling with GIS. *Geographical information systems*, 207–217.

Horton, R., *et al*. 2015. New York City panel on climate change 2015 report chapter 2: sea level rise and coastal storms. *Annals of the New York Academy of Sciences*, 1336 (1), 36–44. doi:10.1111/nyas.12593

Hsu, Y.C., *et al*., 2016. An investigation of DEM resolution influence on flood inundation simulation. *Procedia Engineering*, 154, 826–834. doi:10.1016/j.proeng.2016.07.435

Hurrell, J.W., 1995. Decadal trends in the North Atlantic oscillation: regional temperatures and precipitation. *Science*, 269, 676–679. doi:10.1126/science.269.5224.676

Jelesnianski, C.P., *et al*., 1992. SLOSH: sea, lake, and overland surges from hurricanes. *NOAA Tech. Rep. NWS*, 48. U.S. Department of Commerce.

Kane, H.H., *et al*. 2015. Critical elevation levels for flooding due to sea-level rise in Hawai'i. *Regional Environmental Change*, 15 (8), 1679–1687. doi:10.1007/s10113-014-0725-6

Kenigson, J.S. and Han, W., 2014. Detecting and understanding the accelerated sea level rise along the east coast of the United States during recent decades. *Journal of Geophysical Research: Oceans*, 119 (12), 8749–8766.

Kleinosky, L.R., *et al*. 2007. Vulnerability of Hampton Roads, Virginia to storm-surge flooding and sea-level rise. *Natural Hazards*, 40 (1), 43–70. doi:10.1007/s11069-006-0004-z

Kopp, R.E., 2013. Does the mid-Atlantic United States sea level acceleration hot spot reflect ocean dynamic variability? *Geophysical Research Letters*, 40 (15), 3981–3985. doi:10.1002/grl.50781

Kress, M.E., *et al*. 2016. Modeling and simulation of storm surge on Staten Island to understand inundation mitigation strategies. *Journal of Coastal Research*, 76 (sp1), 149–161. doi:10.2112/SI76-013

Lempert, R., 2018. Reducing risks through adaptation actions. *In*: D.R. Reidmiller, *et al*., eds. *Impacts, risks, and adaptation in the United States: fourth national climate assessment, volume II*. Washington, DC: U.S. Global Change Research Program, 1309–1345. doi:10.7930/NCA4.2018.CH28

Leon, J.X., *et al*. 2014. Incorporating DEM uncertainty in coastal inundation mapping. *PLoS ONE*, 9 (9), 1–12. doi:10.1371/journal.pone.0108727

Li, X., *et al*. 2009. GIS analysis of global impacts from sea level rise. *Photogrammetric Engineering and Remote Sensing*, 75 (7), 807–818. doi:10.14358/PERS.75.7.807

Lin, N., *et al*. 2012. Physically based assessment of hurricane surge threat under climate change. *Nature Climate Change*, 2 (6), 462. doi:10.1038/nclimate1389

Loder, N., *et al*. 2009. Sensitivity of hurricane surge to morphological parameters of coastal wetlands. *Estuarine, Coastal and Shelf Science*, 84 (4), 625–636. doi:10.1016/j.ecss.2009.07.036

Lombard, A., *et al*., 2005. Contribution of thermal expansion to present-day sea level change revisited. *Global and Planetary Change*, 47, 1–16. doi:10.1016/j.gloplacha.2004.11.016

Lowe, J.A., *et al*. 2001. Changes in the occurrence of storm surges around the United Kingdom under a future climate scenario using a dynamic storm surge model driven by the Hadley Centre climate models. *Climate Dynamics*, 18 (3–4), 179–188. doi:10.1007/s003820100163

Lowe, J.A. and Gregory, J.M., 2005. The effects of climate change on storm surges around the United Kingdom. *Philosophical Transactions of the Royal Society of London A Mathematical, Physical and Engineering Sciences*, 363 (1831), 1313–1328. doi:10.1098/rsta.2005.1570

Luettich, R.A., Jr., *et al*., 1992. ADCIRC: an advanced three-dimensional circulation model for shelves, coasts, and estuaries. Report 1. Theory and methodology of ADCIRC-2DDI and ADCIRC-3DL. No. CERC-TR-DRP-92-6. Vicksburg, MS.

Maloney, M.C. and Preston, B.L., 2014. A geospatial dataset for US hurricane storm surge and sea-level rise vulnerability: development and case study applications. *Climate Risk Management*, 2, 26–41. doi:10.1016/j.crm.2014.02.004

Mancini, F., *et al*. 2013. Using unmanned aerial vehicles (UAV) for high-resolution reconstruction of topography: the structure from motion approach on coastal environments. *Remote Sensing*, 5 (12), 6880–6898. doi:10.3390/rs5126880

Maune, D.F. and Nayegandhi, A., ed., 2018. *Digital elevation model technologies and applications: the DEM user manual*. 3rd ed. Bethesda, MD: American Society for Photogrammetry and Remote Sensing.

McBratney, A.B., *et al*. 2003. On digital soil mapping. *Geoderma*, 117 (1–2), 3–52. doi:10.1016/S0016-7061(03)00223-4

McInnes, K.L., *et al*. 2003. Impact of sea-level rise and storm surges in a coastal community. *Natural Hazards*, 30 (2), 187–207. doi:10.1023/A:1026118417752

McInnes, K.L., *et al*. 2013. An assessment of current and future vulnerability to coastal inundation due to sea-level extremes in Victoria, southeast Australia. *International Journal of Climatology*, 33 (1), 33–47. doi:10.1002/joc.3405

Milne, G.A., *et al*. 2009. Identifying the causes of sea-level change. *Nature Geoscience*, 2 (7), 471–478. doi:10.1038/ngeo544

Murty, T.S., *et al*. 1986. The storm surge problem in the Bay of Bengal. *Progress in Oceanography*, 16 (4), 195–233. doi:10.1016/0079-6611(86)90039-X

Nelson, A., *et al*. 2009. DEM production methods and sources. *In*: T. Hengl and H.I. Reuter, eds. *Geomorphometry: concepts, software, and applications*. Amsterdam: Elsevier, 65–85.

Nerem, R.S. and Mitchum, G.T., 2001. Sea level change. *In*: L. Fu and A. Cazenave, eds. *Satellite altimetry and earth sciences: a handbook of techniques and applications*. San Diego, CA: Academic Press, 329–349.

Neumann, J.E., *et al*. 2010. Assessing sea-level rise impacts: a GIS-based framework and application to coastal New Jersey. *Coastal Management*, 38 (4), 433–455. doi:10.1080/08920753.2010.496105

NOAA, 2018. Tides and Currents. https://tidesandcurrents.noaa.gov/sltrends/sltrends_station.shtml?id=8531680. Accessed 23 March 2018.

NYC Department of Parks and Recreation, 2010. https://data.cityofnewyork.us/Environment/Landcover-Raster-Data-2010-3ft-Resolution/9auy-76zt. Accessed 1 March 2019

Nyquist, H., 1928. Certain topics in telegraph transmission theory. *Transactions of the American Institute of Electrical Engineers*, 47 (2), 617–644. doi:10.1109/T-AIEE.1928.5055024

Openshaw, S., 1977. A geographical solution to scale and aggregation problems in region building, partitioning and spatial modeling. *Transactions of the Institute of British Geographers*. 459–472.

Openshaw, S., 1983. *The modifiable areal unit problem*. Concepts and Techniques in Modern Geography No. 38. Norwich, England: Geobooks.

Orton, P., *et al*. 2015. New York City panel on climate change 2015 report chapter 4: dynamic coastal flood modeling. *Annals of the New York Academy of Sciences*, 1336 (1), 56–66. doi:10.1111/nyas.12589

Parris, A., *et al*., 2012. Global sea level rise scenarios for the US national climate assessment. NOAA Tech Memo OAR CPO-1, 37 pp.

Patrick, L., *et al*. 2015. New York City panel on climate change 2015 report chapter 3: static coastal flood mapping. *Annals of the New York Academy of Sciences*, 1336 (1), 45–55. doi:10.1111/nyas.12590

Pielke, R.A., Jr., 1999. Nine fallacies of floods. *Climatic Change*, 42, 413–438. doi:10.1023/A:1005457318876

Poulter, B. and Halpin, P.N., 2008. Raster modeling of coastal flooding from sea-level rise. *International Journal of Geographical Information Science*, 22 (2), 167–182. doi:10.1080/13658810701371858

Rabus, B., *et al*. 2003. The shuttle radar topography mission — a new class of digital elevation models acquired by spaceborne radar. *Photogrammetric Engineering and Remote Sensing*, 57 (4), 241–262. doi:10.1016/S0924-2716(02)00124-7

Rodriguez, E., *et al*., 2005. An assessment of the SRTM topographic products. Pasadena, CA: Jet Propulsion Laboratory Technical Report JPLD-31639, 143 p.

Saksena, S. and Merwade, V., 2015. Incorporating the effect of DEM resolution and accuracy for improved flood inundation mapping. *Journal of Hydrology*, 530, 180–194. doi:10.1016/j.jhydrol.2015.09.069

Schmid, K., *et al*. 2014. Mapping and portraying inundation uncertainty of bathtub-type models. *Journal of Coastal Research*, 30 (3), 548–561. doi:10.2112/JCOASTRES-D-13-00118.1

Seenath, A., *et al*., 2016. Hydrodynamic versus GIS modelling for coastal flood vulnerability assessment: which is better for guiding coastal management? *Ocean & Coastal Management*, 120, 99–109. doi:10.1016/j.ocecoaman.2015.11.019

Shannon, C.E., 1949. Communication in the presence of noise. *Proceedings of the Institute of Radio Engineers*, 37, 10–21.

Shean, D.E., *et al*., 2016. An automated, open-source pipeline for mass production of digital elevation models (DEMs) from very-high-resolution commercial stereo satellite imagery. *ISPRS Journal of Photogrammetry and Remote Sensing*, 116, 101–117. doi:10.1016/j.isprsjprs.2016.03.012

Shepard, C.C., *et al*. 2012. Assessing future risk: quantifying the effects of sea level rise on storm surge risk for the southern shores of Long Island, New York. *Natural Hazards*, 60 (2), 727–745. doi:10.1007/s11069-011-0046-8

Spaete, L.P., *et al*. 2011. Vegetation and slope effects on accuracy of a LiDAR-derived DEM in the sagebrush steppe. *Remote Sensing Letters*, 2 (4), 317–326. doi:10.1080/01431161.2010.515267

Spearman, C., 1904. The proof and measurement of association between two things. *American Journal of Psychology*, 15 (1), 72–101. doi:10.2307/1412159

Strauss, B., *et al*. 2012. Tidally-adjusted estimates of topographic vulnerability to sea level rise and flooding for the contiguous United States. *Environmental Research Letter*, 7 (1), 1–12. doi:10.1088/1748-9326/7/1/014033

Su, J. and Bork, E., 2006. Influence of vegetation, slope, and lidar sampling angle on DEM accuracy. *Photogrammetric Engineering & Remote Sensing*, 72 (11), 1265–1274. doi:10.14358/PERS.72.11.1265

Sweet, W.V., *et al*. 2013. Section 6: Hurricane Sandy inundation probabilities today and tomorrow. *Bulletin of the American Meteorological Society*, 94, S17–S20.

Sweet, W.V., *et al*., 2017. Sea level rise. *In*: D.J. Wuebbles, *et al*., eds. *Climate science special report: fourth national climate assessment, volume I*. Washington, DC: U.S. Global Change Research Program, 333–363. doi:10.7930/J0VM49F2

Talke, S.A., *et al*. 2014. Increasing storm tides in New York Harbor, 1844–2013. *Geophysical Research Letters*, 41 (9), 3149–3155. doi:10.1002/2014GL059574

Titus, J.G., *et al*. 1987. Greenhouse effect, sea level rise, and coastal drainage systems. *Journal of Water Resources Planning and Management*, 113 (2), 216–227. doi:10.1061/(ASCE)0733-9496-(1987)113:2(216)

Titus, J.G. and Richman, C., 2001. Maps of lands vulnerable to sea level rise: modeled elevations along the US Atlantic and Gulf coasts. *Climate Research*, 18 (3), 205–228. doi:10.3354/cr018205

Trenberth, K.E. and Shea, D.J., 2006. Atlantic hurricanes and natural variability in 2005. *Geophysical Research Letters*, 33, 12. doi:10.1029/2006GL026894

Van de Sande, *et al*., 2012. Sensitivity of coastal flood risk assessments to digital elevation models. *Water*, 4, 568–579. doi:10.3390/w4030568

Wallentin, G. and Car, A., 2013. A framework for uncertainty assessment in simulation models. *International Journal of Geographical Information Science*, 27 (2), 408–422. doi:10.1080/13658816.2012.715163

Walsh, K.J., *et al*., 2012. Climate change impacts on tropical cyclones and extreme sea levels in the South Pacific—A regional assessment. *Global and Planetary Change*, 80, 149–164. doi:10.1016/j.gloplacha.2011.10.006

Wang, C. and Zhang, L., 2013. Multidecadal ocean temperature and salinity variability in the tropical North Atlantic: linking with the AMO, AMOC, and subtropical cell. *Journal of Climate*, 26 (16), 6137–6162. doi:10.1175/JCLI-D-12-00721.1

Wechsler, S.P., 2007. Uncertainties associated with digital elevation models for hydrologic applications: a review. *Hydrology and Earth System Sciences*, 11 (4), 1481–1500. doi:10.5194/hess-11-1481-2007

Wechsler, S.P. and Kroll, C.N., 2006. Quantifying DEM uncertainty and its effect on topographic parameters. *Photogrammetric Engineering & Remote Sensing*, 72 (9), 1081–1090. doi:10.14358/PERS.72.9.1081

West, H., *et al*. 2018. Exploring the sensitivity of coastal inundation modelling to DEM vertical error. *International Journal of Geographical Information Science*, 32 (6), 1172–1193. doi:10.1080/13658816.2018.1444165

Wilson, J.P., 2012. Digital terrain modeling. *Geomorphology*, 137 (1), 107–121. doi:10.1016/j.geomorph.2011.03.012

Winter, B., *et al*. 2018. Sources of uncertainty in a probabilistic flood risk model. *Natural Hazards*, 91 (2), 431–446. doi:10.1007/s11069-017-3135-5

Wong, P.P., *et al*., 2014. *Climate change 2014: impacts, adaptation, and vulnerability. part A: global and sectoral aspects. Contribution of working group II to the fifth assessment report of the intergovernmental panel on climate change*. C.B. Field, *et al*., eds. Cambridge, UK: Cambridge University Press, 361–409

Woolpert, 2014. *New York CMGP Sandy 0.7M NPS lidar*. Ohio: Woolpert Dayton. https://coast.noaa.gov/htdata/lidar1_z/geoid12b/data/4920/supplemental/Lidar_Rpt_NYSandy_Lidar_October_2014.pdf [Accessed 28 March 2018].

Yin, J., *et al*. 2009. Model projections of rapid sea-level rise on the northeast coast of the United States. *Nature Geoscience*, 2 (4), 262. doi:10.1038/ngeo462

Yin, J., *et al*. 2010. Spatial variability of sea level rise in twenty-first century projections. *Journal of Climate*, 23 (17), 4585–4607. doi:10.1175/2010JCLI3533.1

Zarrilli, D., 2015. *Appeal of FEMA's preliminary flood insurance rate maps for New York City*. Technical report. New York: Mayor's Office of Recovery and Resiliency.

Zhang, K., 2011. Analysis of non-linear inundation from sea-level rise using LIDAR data: a case study for South Florida. *Climatic Change*, 106 (4), 537–565. doi:10.1007/s10584-010-9987-2

Zhang, K., *et al*. 2013. Comparison of three methods for estimating the sea level rise effect on storm surge flooding. *Climatic Change*, 118 (2), 487–500. doi:10.1007/s10584-012-0645-8